Results in Physics 19 (2020) 103421

Contents lists available at ScienceDirect

Results in Physics

journal homepage: www.elsevier.com/locate/rinp

Quantum control of an optically dense atomic medium: Pulse shaping in a V-type three-level system

N. Boutabba [a,*], H. Eleuch [b,c,d]

[a] Fatima College of Health Sciences, Institute of Applied Technology, Abu Dhabi, United Arab Emirates
[b] Department of Applied Physics and Astronomy, University of Sharjah, Sharjah, United Arab Emirates
[c] Department of Applied Sciences and Mathematics, Abu Dhabi University, Abu Dhabi, United Arab Emirates
[d] Institute for Quantum Science and Engineering, Texas A&M University, College Station, TX 77843, USA

ARTICLE INFO

Keywords:
Atomic population inversion
Three-level atom
Quantum control

ABSTRACT

In this paper, we suggest a straight-forward technique to control the atomic population inversion in a three-level dense medium based on the pulse shaping with a phase-jump. A strong stokes field and two weak probe fields excite the atomic medium via the V-type configuration. First, we reveal that the atomic population inversion is accomplished under a shaped pulse. Second, we show that this is significantly improved by including a phase-jump in the pulse profile. Finally, we suggest a typical combined shape and phase in order to control the dynamics of the atomic population inversion.

Introduction

The interaction of quantum systems with light has drawn considerable interest due to their significant impact in several fields of Physics [1]. In fact, these interactions form the basis of a wide range of applied technology, such as laser beams, diodes [2], atomic clocks[3,4], nanolasers [5], single photon transistors [6,7], nanophotonics [8] and all optical modulators and sensors [9]. Furthermore, light-matter interaction based on quantum coherence lays the foundation for studies in quantum optics[10–14]. In fact, coherent control of light is considered as one of the main sources of quantum interference and aims to enhance non-linear optical processes in spectroscopy and microscopy [15,16]. In the field of atomic and molecular optics, rapid progress has emerged thanks to the coherent control of light with pulse shaping [17–19]. In fact, pulse shaping methods allow the generation of designable optical wave-forms made according to user specifications. Based on pulse shaping, single beams as well as coherent anti-Stokes Raman scattering techniques called (CARS) allow chemically selective non-linear spectroscopy [20]. This has given rise to many new directions, such as quantum computing and data communications with terabit/s [21]. The target of pulse shaping is the control of amplitude, frequency, and phase. One pertinent example is the Laser pulse shaping via the chirp frequency technique, used in [22] to control the excitation probability of a two-level system. In that study, the dependence of the population of the upper energy level on the chirp was investigated for different radiation intensities and pulse durations. Nonetheless, pulse shaping and developments in femto-second pulse techniques[19] have a significant effect on the advancement of many fields such as nuclear magnetic resonance (NMR)[23–25], spectroscopy[26], non-linear fiber optics [27–29], and high-energy physics[30,17,31–33]. Additionally, pulse shaping techniques provide a significant insight into an interdisciplinary approach leading to important results in biology [34,35].

In this work, we consider a classical multi-level atom, where we apply a strong light pulse and two weak probe lights to excite Rubidium atoms in a V-type configuration. We show that, by manipulating the shape of the stokes field, we realize the atomic population inversion. In addition, we enhance it by applying a phase-jump to the control field. This paper is organized as follows: In the first section, we present the model. In the second section, we analyse and describe our system in terms of the density matrix formalism, then we present the results in the third section followed by concluding remarks.

Model

In this model, a typical three-level atomic medium with a V-type configuration is considered (Fig. 1). The different levels denoted by (m, l) where ($m, l = 1, 3$) are coupled to the corresponding (m, l) fields as follows: the field E_c with a Rabi frequency Ω_c drives the level $|2\rangle$ to the

* Corresponding author.
E-mail address: n_boutabba@yahoo.fr (N. Boutabba).

https://doi.org/10.1016/j.rinp.2020.103421
Received 17 July 2020; Received in revised form 13 September 2020; Accepted 17 September 2020
Available online 24 September 2020

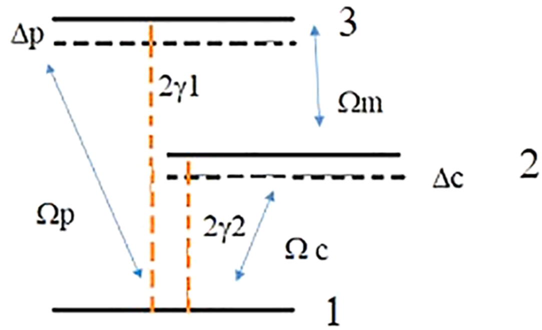

Fig. 1. The energy diagram of a three-level V-type medium.

level $|1\rangle$ while the weak probe field couples the level $|3\rangle$ to the level $|1\rangle$. A weak field E_m couples the level pairs $|3\rangle$ to $|2\rangle$. This atomic scheme can be experimentally realized by a Rb^{87} atom with $5S_{1/2}$, F = 1, m = 1, $5P_{1/2}$, F = 1, m = 0 and $5S_{1/2}$, F = 2, m = 1 representing the $|1\rangle, |2\rangle, |3\rangle$ respectively [36]. The frequency detunings Δ_c and Δ_p correspond respectively to $\omega_c - \omega_{21}$ and $\omega_p - \omega_{31}$. The radiative decay rates taking into account in this scheme are $\gamma_{1,2}$ from the higher level$|3\rangle$ to $|1\rangle$ and $|2\rangle$ to $|1\rangle$. This is illustrated in Fig. 1. The Hamiltonian under the rotating wave approximation is given by:

$$H = \Delta_p|3\rangle\langle 3| + \Delta_c|2\rangle\langle 2| - (\Omega_c|2\rangle\langle 1| + \Omega_c^*|1\rangle\langle 2| + \Omega_p|3\rangle\langle 1| + \Omega_m|3\rangle\langle 2|) \quad (1)$$

Where the detunings of the probe and coupling fields are given by $\Delta_p = \omega_{31} - \omega_p$ and $\Delta_c = \omega_{21} - \omega_c$ respectively. The temporal evolution of the system is governed by the master equations of the Hermitian density matrix as:

$$\sum_{i,j} \frac{\partial \rho_{ij}}{\partial t} = 1. \quad (2)$$

And:

$$\frac{d}{dt}\rho_{22} = -2\gamma_2\rho_{22} + i\Omega_c(\rho_{12} - \rho_{21}) + i\Omega_m(\rho_{32} - \rho_{23}) \quad (3)$$

$$\frac{d}{dt}\rho_{33} = -2\gamma_1\rho_{33} + i\Omega_p(\rho_{13} - \rho_{31}) + i\Omega_m(\rho_{23} - \rho_{32}) \quad (4)$$

And where the density matrix non-diagonal elements are given by:

$$\frac{d}{dt}\varrho_{21} = -(\gamma_2 + i\Delta_c)\rho_{21} + i\Omega_c(\rho_{11} - \rho_{22}) \quad (5)$$

$$-i\Omega_p\rho_{23} + i\Omega_m\rho_{31}$$

$$\frac{d}{dt}\varrho_{31} = -(\gamma_1 + i\Delta_p)\rho_{31} + i\Omega_p(\rho_{11} - \rho_{33}) \quad (6)$$

$$-i\Omega_c\rho_{32} + i\Omega_m\rho_{21}$$

$$\frac{d}{dt}\varrho_{32} = -(\gamma_1 + \gamma_2 - i\Delta_c + i\Delta_p)\rho_{32} \quad (7)$$

$$+ i\Omega_p\rho_{12} - i\Omega_c\rho_{31} + i\Omega_m(\rho_{22} - \rho_{33})$$

To analyse the density matrix, we consider the rubidium atom Rb^{87} where all Rabi frequencies are scaled by the decay rate γ_1 . Thus, $\gamma_1 = 1$, $\gamma_2 = 3$, $\Omega_p = 5$ and $\Omega_m = 1$. We investigate in the next section the laser inversion by analyzing the atomic population inversion.

Optical field

The control field is considered as a beam of the general form: $\Omega_c \propto f(t) e^{I\phi}$ where f(t) defines the light shape and ϕ is the fast phase of the laser pulse. Now, we first consider a pulse with a temporal super-Gaussian shape where the light varies between the smooth and the pure flat-top shape. In fact, the analysis of the propagation of super-Gaussian field distributions is based on the super-Gaussian function that defines a whole family of field distributions with increasingly sharp edges ranging from strictly Gaussian to uniform flat-top. Here, the control field is defined as one whose profile follows the mathematical function:

$$f(t) = f_0\exp(-\alpha t^p) \quad (8)$$

$$= f_0\exp\left(-\left(\frac{t}{\sigma}\right)^p\right)$$

where α is a variable and p is the order of the super-Gaussian. In the case of a second order temporal Gaussian beam, the Gaussian spectrum is proportional to pulse rise time σ, and that the time-bandwidth product is calculated using the temporal and spectral FWHM widths in intensity. The general form of ϕ depends on the time and the spatial coordinates where the angular frequency of the pulse and the wave number are related to ϕ through the first derivative [37]. Finally, it is worth noting that experimentally, the pulse shaping and the processing of desirable optical wave-forms are possible via many techniques [38–41]. Among them, the micro-lithographic pattern technique [42], the spatial light modulators programs [43], the acousto-optic modulators [44], the deformable mirrors [45] etc. Most of these experiments use a spatial light modulator to realize tailored waveforms, while most theoretical work takes on a perfectly modulated pulse, whose electrical field depends only on time or frequency. A promising technique to realize pulse shaping in a V-type three-level system is reported in [46]. The authors, investigated the space–time coupling in femtosecond pulse shaping experimentally. They addressed experimentally the effects of space–time coupling on non-linear interactions, namely, second harmonic generation. Besides, the effects of space–time coupling on the interaction of laser pulses with a three-level V-type atomic system as well as resonant diatomic molecules were reported based on a simulation, which could open the way for experimental realization based on space–time couplings. Within the next section, we examine the time evolution of the atomic population inversion with and without phase for different fields of light, denoted by:

$$W = \rho_{33}(t) - \rho_{22}(t) \quad (9)$$

where t is normalized in units of τ and W is obtained by solving numerically the master equations above.

Atomic population inversion and phase-jump

To analyse the atomic population dynamics as well as the optical control of the laser inversion, we consider the rubidium atom Rb^{87} where all Rabi-frequencies are scaled by the decay rate γ_1 . Thus, $\gamma_1 = 1$, $\gamma_2 = 3, \Omega_p = 5$ and $\Omega_m = 1$. The time t in the reported figures has units of τ, where $\tau = \frac{1}{\gamma_1}$ is the Rubidium lifetime and γ_1 is the decay rate [47]. In Fig. 2 and 4, the Gaussian pump laser is shown for different shapes and orders related respectively to the parameters α and p, while the atomic population inversion is reported in Fig. 4 and 5. In Fig. 2, we note that for higher p, the light pulse is almost flat on the top.

Fig. 3 reports the atomic population dynamics $\rho_{33} - \rho_{22}$ corresponding to the different orders of the pump pulse. The population inversion between the levels $|3\rangle$ and $|2\rangle$ is realized after t = 1.2 for the flat-top beam first, than for lower orders. For the second-order beam, we notice an inversion of population after the normalized time t = 2. Fig. 4 shows the Gaussian control field pulse for different pulse rise time by varying α. Respectively, in Fig. 5, the atomic population dynamics $\rho_{33} - \rho_{22}$ is reported. In comparison with the results reported in Fig. 3, we deduce that the atomic population dynamics between the levels $|3\rangle$ and $|2\rangle$ is almost the same for $t \in]0, +1[$ in units of τ.

This means that the input Gaussian pulse order has no effect on the atomic dynamics at the beginning. While the pulse rise time variation contributes to more splitting between the atomic population dynamics

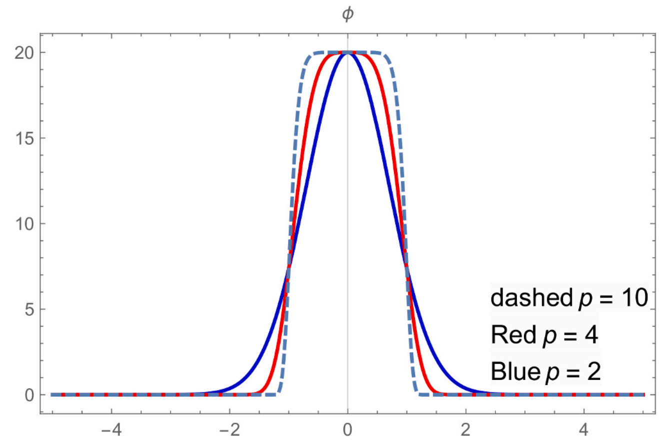

Fig. 2. The pump light shape: the pulse profiles of a super-Gaussian field of orders p = 2,4 and 10.

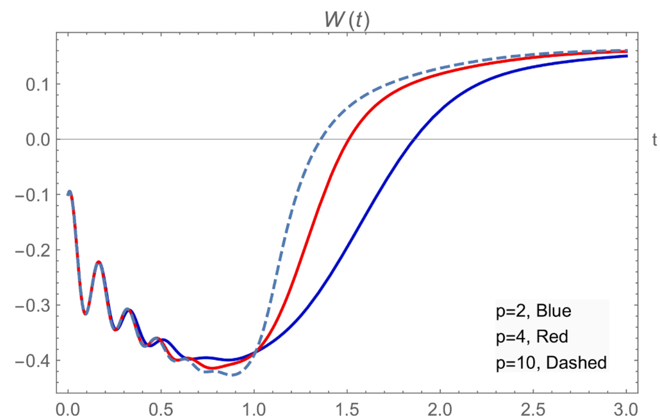

Fig. 3. $\rho_{33} - \rho_{22}$ dynamics for a Gaussian control light beam with various orders. All the normalized parameters are taken for a Rb^{87}.

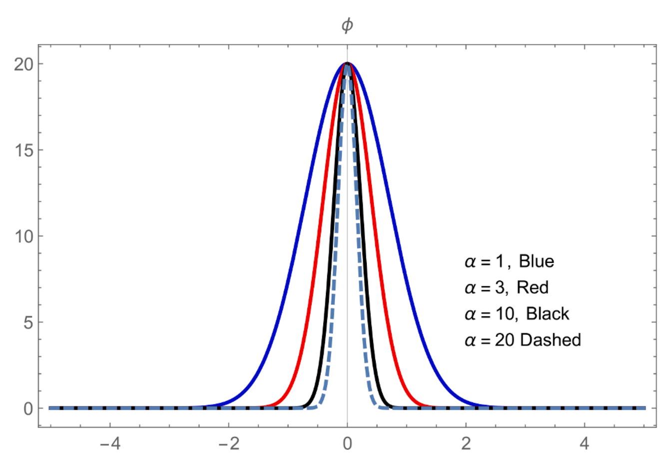

Fig. 4. The Gaussian light shape for different widths.

in Fig. 5. $\rho_{33} - \rho_{22}$ dynamics starts to increase as soon as t is greater than 0.25 in Fig. 5. We clearly get an enhancement of the population inversion for a light pulse approaching a Lorentzian input shape ($\alpha = 20$), for small pulse rise time. This means that for a fast cycle pulse, the population inversion is enhanced. By combining both effects of the fast pulse rise time and the temporal super-Gaussian order we consider a Rabi field $\Omega_c = 20\xi$ where $\xi = e^{-\alpha_2 t^p}$, with p = 2 and $\alpha_2 = 10$. In addition, we consider a phase $\phi = \phi_t$. The results of this input pulse on the population

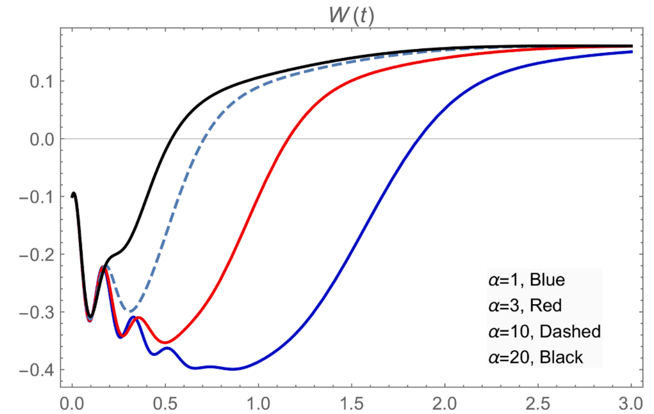

Fig. 5. $\rho_{33} - \rho_{22}$ dynamics for different Gaussian widths. All the parameters are taken for a Rb^{87}.

dynamics is reported in Fig. 6, where different colors refer to different control fields.

In Figs. 6 and 7, the black curve designs the case of a constant coupling field $\Omega_c = 20$. The dashed one considers a Gaussian shape pulse $\Omega_c = 20\xi$ (for p = 2) without a phase, while the blue curve is for a Gaussian shape (p = 2) with a phase such as:$\Omega_c = 20\xi e^{-i\theta}$ and $\theta = \pi(1 + tanh(t))/2 + sech(t)^2$. Finally, the red curve is for a control field with a phase as: $\Omega_c = 20e^{-i\phi}$ where $\phi = \pi(1 + tanh(t))/2$. Here, we note that the combined pulse rise time and order considered for the blue and the dashed cases, realize the inversion of the atomic population. In the meantime, all considered fields, with and without ξ, change the coherence of the atomic medium considerably. (see ρ_{31} dynamics for different pulses with phases in Fig. 7). Compared to previous cases in Figs. 4 and 5, we conclude that taking into account the above-identified phases is an efficient way of realizing and improving the population inversion. Now, we suggest a phase-jump of the form:

$$\phi(t) = cos(\alpha_1 t). \tag{10}$$

α_1 is the frequency of the variable phase. In addition, we combine this phase to a pulse amplitude with a complicated sec–hyperbolic form [48]. The total field is written as

$$\Omega_{cj} = 20(sech\alpha t + sech(\alpha t + 3))e^{-0.5t^2 - i\phi(t)}. \tag{11}$$

This typical phase allows the control of the atomic population inversion as it is demonstrated in Fig. 8. In fact, for a constant control field no population inversion is realized (see the dashed curve), only a consideration of a Gaussian shape allows the atomic population inversion to appear: see the blue curve where the atomic population inversion

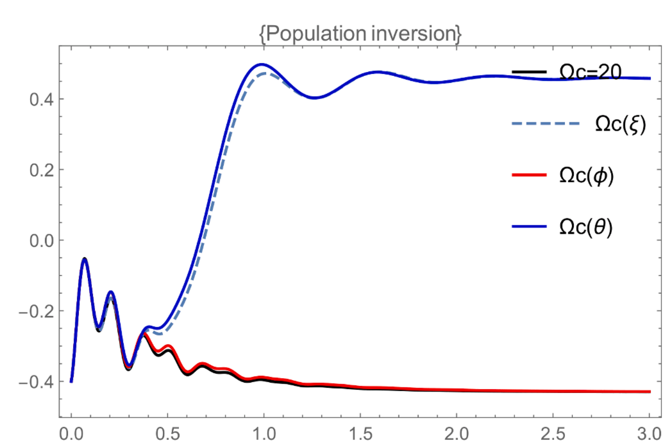

Fig. 6. Population inversion. All the parameters are taken for a Rb^{87}.

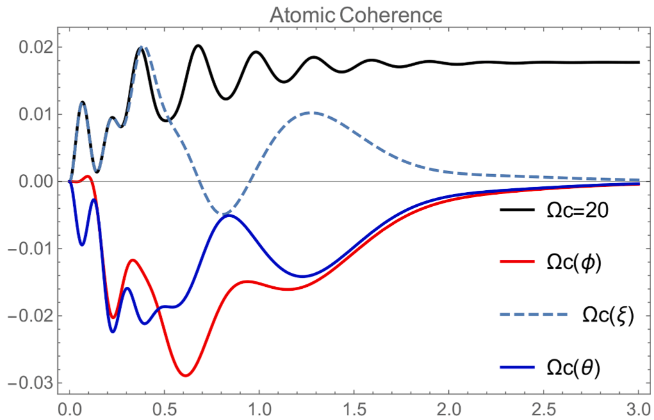

Fig. 7. Atomic coherence. All the parameters are taken for a Rb^{87}.

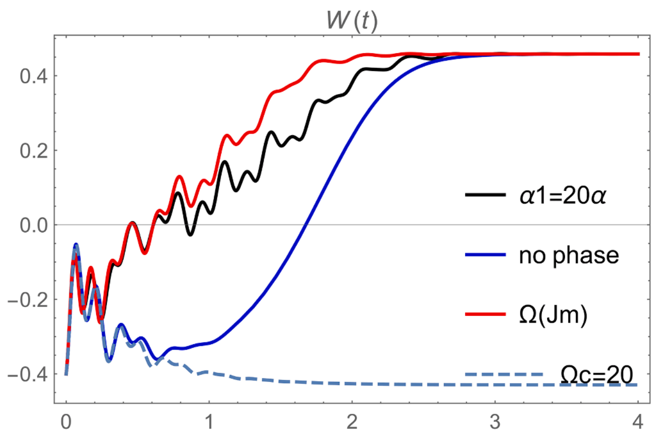

Fig. 8. Phase-Jump control of the atomic inversion.

is reported for a control field with a Gaussian shape and without a phase. However, this population inversion is realized after a certain delay in time t (t is in units of τ). As it is shown in the black curve of Fig. 8, we combine a Gaussian pulse shape of order 2 (p = 2) with a phase-jump. The introduction of the suggested phase-jump enhances considerably the atomic population inversion. Further control of the atomic population dynamics is obtained for a sec-hyperbolic complicated pulse with a phase-jump as it is shown by the red curve in Fig. 8. Finally, the control field pulse denoted by:

$$\Omega_{cj} = 20(sech\alpha t + sech(\alpha t + 3))e^{-0.5t^2 - i\phi(t)} \tag{12}$$

gives the best results as seen in the red curve, in which the complicated form is coupled with a phase-jump created by a very fast time pulse.

Conclusion

In this paper, we investigate the effect of the light pulse shape on the control of a three-level atomic system. We consider a Rb^{87} medium interacting with three electromagnetic fields. It is a structure of a V-type configuration where a weak beam of light propagates in the medium and interacts with a strong control field. By exploring the coupling rate equations in the density matrix approach, we show that we can control the atomic population dynamics by manipulating the light pulse shape. In fact, by applying various super-Gaussian beams with and without phase, we are able to realize the atomic population inversion and to control the population dynamics. Furthermore, through selecting a specific sec-hyperbolic pulse shape with a phase-jump, the population inversion is greatly enhanced.

Declaration of Competing Interest

The authors declare that they have no known competing financial interests or personal relationships that could have appeared to influence the work reported in this paper.

References

[1] Yang J, Lu Y. Black phosphorus: Light-matter interactions and potential applications, in: 2D Materials for Photonic and Optoelectronic Applications, Elsevier; 2020. p. 159–73.

[2] Altorio M, Sidorenkov L, Gautier R, Savoie D, Landragin A, Geiger R. Accurate trajectory alignment in cold-atom interferometers with separated laser beams. Phys Rev A 2020;101(3):033606.

[3] Boyd MM, Black AT, Patton BR, Zhu M. Integrated optical detection for atomic clocks and sensors, uS Patent 10,535,981 (Jan. 14 2020).

[4] Clements E, Kim M, Cui K, Hankin A, Brewer S, Chen J-S, Leibrandt D, Hume D. Correlation spectroscopy between two 27 al+ quantum-logic clocks. Bull Am Phys Soc.

[5] Geng Q, Wang D, Chen P, Chen S-C. Ultrafast multi-focus 3-d nano-fabrication based on two-photon polymerization. Nat Commun 2019;10(1):1–7.

[6] Yang H, Yan Y, Wu X, Liu Y, Chen Q, Zhang G, Chen S, Chen H, Guo T. Multilevel vertical photonic memory transistor based on organic semiconductor/inorganic perovskite quantum dots blends. J Mater Chem C.

[7] Cho SW, Kwon SM, Lee M, Jo J-W, Heo JS, Kim Y-H, Cho HK, Park SK. Multi-spectral gate-triggered heterogeneous photonic neuro-transistors for power-efficient brain-inspired neuromorphic computing. Nano Energy 2019;66:104097.

[8] Koshelev K, Kruk S, Melik-Gaykazyan E, Choi J-H, Bogdanov A, Park H-G, Kivshar Y. Subwavelength dielectric resonators for nonlinear nanophotonics. Science 2020;367(6475):288–92.

[9] Lee M, Friebe K, Fioretto DA, Schüppert K, Ong FR, Plankensteiner D, Torggler V, Ritsch H, Blatt R, Northup TE. Ion-based quantum sensor for optical cavity photon numbers. Phys Rev Lett 2019;122(15):153603.

[10] Chen Y-H, Xia Y, Chen Q-Q, Song J. Fast and noise-resistant implementation of quantum phase gates and creation of quantum entangled states. Phys Rev A 2015;91(1):012325.

[11] Kang Y-H, Chen Y-H, Shi Z-C, Song J, Xia Y. Fast preparation of w states with superconducting quantum interference devices by using dressed states. Phys Rev A 2016;94(5):052311.

[12] Chen Y-H, Xia Y, Chen Q-Q, Song J. Shortcuts to adiabatic passage for multiparticles in distant cavities: applications to fast and noise-resistant quantum population transfer, entangled states' preparation and transition. Laser Phys Lett 2014;11(11):115201.

[13] Chen Y-H, Shi Z-C, Song J, Xia Y, Zheng S-B. Accelerated and noise-resistant generation of high-fidelity steady-state entanglement with rydberg atoms. Phys Rev A 2018;97(3):032328.

[14] Boutabba N. Kerr-effect analysis in a three-level negative index material under magneto cross-coupling. J Opt 2018;20(2):025102.

[15] Dudovich N, Oron D, Silberberg Y. Single-pulse coherently controlled nonlinear raman spectroscopy and microscopy. Nature 2002;418(6897):512–4.

[16] Silberberg Y. Quantum coherent control for nonlinear spectroscopy and microscopy. Annu Rev Phys Chem 2009;60:277–92.

[17] Maroju PK, Grazioli C, Di Fraia M, Moioli M, Ertel D, Ahmadi H, et al. Attosecond pulse shaping using a seeded free-electron laser. Nature 2020;578(7795):386–91.

[18] Allgaier M, Ansari V, Donohue JM, Eigner C, Quiring V, Ricken R, Brecht B, Silberhorn C. Pulse shaping using dispersion-engineered difference frequency generation. Phys Rev A 2020;101(4):043819.

[19] Goswami D. Optical pulse shaping approaches to coherent control. Phys Rep 2003;374(6):385–481.

[20] Pestov D, Murawski RK, Ariunbold GO, Wang X, Zhi M, Sokolov AV, et al. Optimizing the laser-pulse configuration for coherent raman spectroscopy. Science 2007;316(5822):265–8.

[21] Hernandez VJ, Du Y, Cong W, Scott RP, Li K, Heritage JP, et al. Spectral phase-encoded time-spreading (spects) optical code-division multiple access for terabit optical access networks. J Lightwave Technol 2004;22(11):2671.

[22] Astapenko V, Romadanovskii M. Excitation of a two-level system by a chirped laser pulse. Laser Phys 2009;19(5):969–73.

[23] Warren WS. Effects of pulse shaping in laser spectroscopy and nuclear magnetic resonance. Science 1988;242(4880):878–84.

[24] Silver M, Joseph R, Hoult D. Selective spin inversion in nuclear magnetic resonance and coherent optics through an exact solution of the bloch-riccati equation. Phys Rev A 1985;31(4):2753.

[25] Sacolick L, Rosen MS, Charvat GL, Rothberg JM, Sarracanie M. Pulse sequences for low field magnetic resonance, uS Patent 10,591,561 (Mar. 17 2020).

[26] Akash MSH, Rehman K. Nuclear magnetic resonance spectroscopy. In: Essentials of pharmaceutical analysis. Springer; 2020. p. 137–46.

[27] Wang Z, Nithyanandan K, Coillet A, Tchofo-Dinda P, Grelu P. Buildup of incoherent dissipative solitons in ultrafast fiber lasers. Phys Rev Res 2020;2(1):013101.

[28] Ding X, Heberle D, Harrington K, Flemens N, Chang W-Z, Birks TA, Moses J. Observation of rapid adiabatic passage in optical four-wave mixing. Phys Rev Lett 2020;124(15):153902.

[29] Stephenson L, Nadlinger D, Nichol B, An S, Drmota P, Ballance T, et al. High-rate, high-fidelity entanglement of qubits across an elementary quantum network. Phys Rev Lett 2020;124(11):110501.

[30] Gui G, Karl R, Thurston J, Johnsen P, Bevis C, Binnie I, Kapteyn H, Murnane M, Liao C-T. Quantum control of high-energy harmonic generation by pulse shaping. Bull Am Phys Soc.
[31] Divitt S, Zhu W, Zhang C, Lezec HJ, Agrawal A. Ultrafast optical pulse shaping using dielectric metasurfaces. Science 2019;364(6443):890–4.
[32] Saxena S, Hawari AI. Digital pulse deconvolution with adaptive shaping for real-time high-resolution high-throughput gamma spectroscopy. Nucl Instrum Methods Phys Res Sec A Acceler Spectr Detect Assoc Equip 2020;954:161288.
[33] Dinar N, Celeste D, Silari M, Varoli V, Fazzi A. Pulse shape discrimination of clyc scintillator coupled with a large sipm array. Nucl Instrum Methods Phys Res Sec A Acceler Spectr Detect Assoc Equip 2019;935:35–9.
[34] Dutta B, Sarkar S, Majhi K, R.Bandopadhyay, Interdisciplinary research of physics in biological field leads the nobel prize 2018; 2020.
[35] Strickland D, Mourou G. Compression of amplified chirped optical pulses. Opt Commun 1985;56(3):219–21.
[36] Marte A, Volz T, Schuster J, Dürr S, Rempe G, Van Kempen E, Verhaar B. Feshbach resonances in rubidium 87: Precision measurement and analysis. Phys Rev Lett 2002;89(28):283202.
[37] Malik HK, Devi L. Relativistic self focusing and frequency shift of super-gaussian laser beam in plasma. Results Phys 2020;103070.
[38] Weiner AM. Ultrafast optical pulse shaping: a tutorial review. Opt Commun 2011; 284(15):3669–92.
[39] Li X, Zhang D, Zhang D, Hao L, Chen H, Wang Z, Zhang Y. Dressing control of biphoton waveform transitions. Phys Rev A 2018;97(5):053830.
[40] Li C, Jiang Z, Zhang Y, Zhang Z, Wen F, Chen H, Zhang Y, Xiao M. Controlled correlation and squeezing in pr 3+: Y 2 sio 5 to yield correlated light beams. Phys Rev Appl 2017;7(1):014023.
[41] Zhang Y, Wang Z, Nie Z, Li C, Chen H, Lu K, Xiao M. Four-wave mixing dipole soliton in laser-induced atomic gratings. Phys Rev Lett 2011;106(9):093904.
[42] Weiner A. Jp heritage, and em kirschner. J Opt Soc Am B 1988;5:1563.
[43] Wefers MM, Nelson KA. Generation of high-fidelity programmable ultrafast optical waveforms. Opt Lett 1995;20(9):1047–9.
[44] Dugan M, Tull J, Warren W. High-resolution acousto-optic shaping of unamplified and amplified femtosecond laser pulses. JOSA B 1997;14(9):2348–58.
[45] Zeek E, Maginnis K, Backus S, Russek U, Murnane M, Mourou G, Kapteyn H, Vdovin G. Pulse compression by use of deformable mirrors. Opt Lett 1999;24(7):493–5.
[46] Frei F, Galler A, Feurer T. Space-time coupling in femtosecond pulse shaping and its effects on coherent control. J Chem Phys 2009;130(3):034302.
[47] Steck DA. Rubidium 87 d line data; 2001.
[48] Rostovtsev YV, Eleuch H, Svidzinsky A, Li H, Sautenkov V, Scully MO. Excitation of atomic coherence using off-resonant strong laser pulses. Phys Rev A 2009;79(6):063833.